

Landscape of stimulation-responsive chromatin across diverse human immune cells

Diego Calderon^{1,18}, Michelle L. T. Nguyen^{2,3,18}, Anja Mezger^{4,5,18}, Arwa Kathiria⁴, Fabian Müller⁴, Vinh Nguyen³, Ninnia Lescano³, Beijing Wu⁴, John Trombetta⁴, Jessica V. Ribado⁴, David A. Knowles^{4,6}, Ziyue Gao^{4,7}, Franziska Blaeschke^{2,3,8}, Audrey V. Parent³, Trevor D. Burt^{9,10}, Mark S. Anderson³, Lindsey A. Criswell^{11,19*}, William J. Greenleaf^{4,12,13,19*}, Alexander Marson^{4,2,3,8,11,13,14,15,16,19*} and Jonathan K. Pritchard^{4,7,17,19*}

A hallmark of the immune system is the interplay among specialized cell types transitioning between resting and stimulated states. The gene regulatory landscape of this dynamic system has not been fully characterized in human cells. Here we collected assay for transposase-accessible chromatin using sequencing (ATAC-seq) and RNA sequencing data under resting and stimulated conditions for up to 32 immune cell populations. Stimulation caused widespread chromatin remodeling, including response elements shared between stimulated B and T cells. Furthermore, several autoimmune traits showed significant heritability in stimulation-responsive elements from distinct cell types, highlighting the importance of these cell states in autoimmunity. Allele-specific read mapping identified variants that alter chromatin accessibility in particular conditions, allowing us to observe evidence of function for a candidate causal variant that is undetected by existing large-scale studies in resting cells. Our results provide a resource of chromatin dynamics and highlight the need to characterize the effects of genetic variation in stimulated cells.

Immune cells respond to stimuli with stereotyped transcriptional programs that enable specialized functions during an immune response. These programs, essential for immune homeostasis, are coordinated by precise interactions of transcription factors that bind genomic sites to influence chromatin landscape and ultimately gene expression. Tight regulation of these programs is required for an appropriate immune response against cancer and infections, and to avoid autoimmunity. Genetic variation in regulatory regions that tune transcriptional programs can contribute to the risk of human autoimmune diseases.

Genome-wide association studies (GWAS) have identified hundreds of genetic variants that contribute to the risk of autoimmunity. Roughly 90% of these signals lie in noncoding regions and thus presumably act by altering gene regulation; however, most of these remain difficult to interpret¹. Several studies have reported enrichment of variants linked to the risk of immune-mediated disorders at key enhancers and cell-specific expression quantitative trait loci (eQTLs), suggesting potential mechanisms by which noncoding variants contribute to disease pathology^{1–7}. Nonetheless, only a minority, perhaps 25%, of GWAS signals can currently be explained through known eQTLs⁸.

Several groups have shown that additional GWAS-eQTL overlap can remain hidden within stimulation-specific functional regions of immune cells^{1,9–13}. Probing these response-specific regional regions can reveal previously undetected disease-associated mechanisms, emphasizing the unique role of stimulation to autoimmunity. For example, our group discovered a stimulation response regulatory element that, when perturbed, resulted in a dysregulated immune response by delaying interleukin-2 receptor subunit alpha (CD25) expression *in vivo*¹⁴. This region harbors a fine-mapped GWAS variant linked to inflammatory bowel disease and type 1 diabetes^{15–17}, thus connecting immune response to autoimmunity. However, these studies have been performed on few stimulated cell types. Thus, we lack a comprehensive view of the effects of stimulation on the chromatin landscape of diverse immune cell types and the role of SNPs in these regions on autoimmune disease.

To address this gap, we developed a resource of chromatin accessibility and gene expression from 25 primary human immune cell types isolated from four human blood donors, in both resting and activated states. Additionally, to further understand chromatin structure in cells important for T cell development, we included six

¹Program in Biomedical Informatics, Stanford University, Stanford, CA, USA. ²Department of Microbiology and Immunology, University of California, San Francisco, San Francisco, CA, USA. ³Diabetes Center, University of California, San Francisco, San Francisco, CA, USA. ⁴Department of Genetics, Stanford University, Stanford, CA, USA. ⁵Department of Medical Biochemistry and Biophysics, Karolinska Institutet, Stockholm, Sweden. ⁶Department of Radiology, Stanford University, Stanford, CA, USA. ⁷Howard Hughes Medical Institute, Stanford University, Stanford, CA, USA. ⁸Innovative Genomics Institute, University of California, Berkeley, Berkeley, CA, USA. ⁹Division of Neonatology, Department of Pediatrics, University of California, San Francisco, San Francisco, CA, USA. ¹⁰Eli and Edythe Broad Center of Regeneration Medicine and Stem Cell Research, University of California, San Francisco, San Francisco, CA, USA. ¹¹Rosalind Russell/Ephraim P. Engleman Rheumatology Research Center, University of California, San Francisco, San Francisco, CA, USA. ¹²Department of Applied Physics, Stanford University, Stanford, CA, USA. ¹³Chan Zuckerberg Biohub, San Francisco, CA, USA. ¹⁴UCSF Helen Diller Family Comprehensive Cancer Center, University of California, San Francisco, San Francisco, CA, USA. ¹⁵Department of Medicine, University of California, San Francisco, San Francisco, CA, USA. ¹⁶Parker Institute for Cancer Immunotherapy, San Francisco, CA, USA. ¹⁷Department of Biology, Stanford University, Stanford, CA, USA. ¹⁸These authors contributed equally: Diego Calderon, Michelle L. T. Nguyen, Anja Mezger. ¹⁹These authors supervised this work: Lindsey A. Criswell, William J. Greenleaf, Alexander Marson, Jonathan K. Pritchard. *e-mail: lindsey.criswell@ucsf.edu; wjg@stanford.edu; alexander.marson@ucsf.edu; pritch@stanford.edu

thymocyte subsets and thymic epithelial cells (TECs) collected from fetal thymus samples.

Overall, we observed features of the chromatin landscape that depend on cell lineage and response to stimulation. Notably, B and T cell subsets shared a significant proportion of these stimulation-responsive chromatin regions. Integrating these data with autoimmune disease GWAS, we found that stimulation-responsive chromatin regions explained significant trait heritability in multiple immune cell types, indicating distinct lineage contributions to autoimmunity. Finally, we leveraged stimulation-responsive chromatin elements and allele-specific imbalance of chromatin accessibility as a functional readout of variants from individual donors to identify autoimmunity-related mechanisms. As proof of concept for the power of this approach, we found evidence of function for a candidate causal SNP that is associated with both rheumatoid arthritis and ulcerative colitis (rs6927172—NC_00006.10:g.138002175C>G), which putatively regulates the expression of *TNFAIP3*.

Results

An atlas of immune cells in resting and stimulated states. To identify the regulatory elements underlying differentiation and stimulation responses in the human immune system, we generated a map of chromatin accessibility and gene expression in resting and stimulated immune cells (Fig. 1a). We isolated 25 specialized immune cell types by flow cytometry from the peripheral blood of up to 4 healthy donors including different subsets of B cells, CD4⁺ T cells, CD8⁺ T cells, $\gamma\delta$ T cells, monocytes, dendritic cells and natural killer (NK) cells (Supplementary Fig. 1 and Supplementary Table 1). Additionally, we collected fetal thymus samples from three donors and isolated a number of thymocyte subsets, including double-positive, double-negative, pre-T double-negative, immature single-positive CD4⁺ and single-positive mature CD4⁺ and CD8⁺ T cells, as well as TECs.

We performed an assay for transposase-accessible chromatin using sequencing (ATAC-seq), which profiles chromatin-accessible regions as a sequencing depth readout¹⁸, and RNA sequencing (RNA-seq) on isolated cell types (Fig. 1b). Details further verifying the quality of the samples can be found in the Supplementary Note. On average, across all resting cell type samples, we identified 36,810 accessible peaks ($q < 0.05$), controlling for the effects of read depth and sample quality.

Unsupervised clustering of ATAC-seq identified distinct chromatin signatures for different lineages (Fig. 1c and Supplementary Fig. 2c). For example, hematopoietic stem cell progenitors (HSCPs) clustered separately from more differentiated immune cell types (data from Corces et al.¹⁹). T cell subsets including CD4⁺, CD8⁺ and $\gamma\delta$ T cells clustered closely together, indicating similar chromatin accessibility profiles for each of them under resting conditions. Circulating mature T cells could be distinguished from their single-positive thymocyte precursors, suggesting further chromatin remodeling in the periphery. Finally, samples generally clustered as expected with published data from the same cell types and, as expected, we observed enrichment of reads at promoters of cell-type-specific genes (Fig. 1c,d).

The same major cell type clusters observed in the chromatin accessibility data were recapitulated when we clustered RNA-seq samples (Supplementary Fig. 2c,d). However, cell type clustering accuracy was higher when using chromatin accessibility than gene expression (mean Hubert and Arabie-adjusted Rand index equal 0.19 and 0.12, respectively), consistent with previous analyses¹⁹.

Identifying immune memory-associated accessible regions.

Taking advantage of the variety of cell types profiled, we quantified changes in chromatin accessibility and gene expression along paths of lymphoid cell differentiation in resting cell types (Fig. 2a and Supplementary Datasets 1 and 2).

Focusing on immune memory formation in different lineages, we found that B and T cells gained accessible chromatin regions as they mature from naïve to memory cells (Fig. 2a,b and Supplementary Note). To discover the factors that potentially drive these chromatin changes, we scanned for transcription factor motifs within accessible regions genome-wide. We observed an enrichment of binding sites for known immune regulators such as JUN–FOS and RUNX3 (Fig. 2c), in addition to increased expression of these transcription factors in memory cells compared to naïve cells (Supplementary Fig. 4b) (ref.²⁰).

Comparing the memory-associated signatures of chromatin accessibility between different lineages, we observed concordant changes between different T cell subsets and a marginal overlap with the accessibility dynamics during B cell memory formation, quantified in terms of Pearson's *R* correlation coefficients as well as overlap between sets of differentially accessible peaks (Fig. 2d,e).

In accordance with previous studies^{21–23}, many genes that are dynamic during memory formation are associated with genomic regions that are putatively regulatory. For example, we found regions exhibiting increased accessibility in memory cells of the B and T lineage compared to naïve cells upstream of the chromatin regulator gene *EED*, which also correlated with increased expression in memory cells (Fig. 2f,h).

To highlight the importance of these regions for understanding autoimmunity, we integrated our estimates of memory-associated accessible regions and differentially expressed genes with a database of GWAS variants²⁴. As an example, we found several regions that increase in accessibility around the *IL23R* gene in effector memory CD8⁺ T cells that contained variants associated with several autoimmune traits (Fig. 2g and Supplementary Fig. 4a). Moreover, *IL23R* was significantly upregulated in effector memory CD8⁺ T cells (Fig. 2h). Thus, dysregulation of immune memory-associated chromatin-accessible regions represents a potentially important effect on autoimmunity.

Stimulation leads to large-scale chromatin changes. Previous studies have shown large-scale chromatin remodeling on stimulation of individual cell types^{9,10,25,26}. We set out to perform a comprehensive analysis of stimulation-dependent chromatin and gene expression changes across a wide range of cell types and lineages. To investigate these effects, we stimulated the majority of the collected cell types *ex vivo* and performed ATAC-seq and RNA-seq.

Our aim was to provide a strong stimulus to each cell type to measure the chromatin dynamics of strongly activated cells. Subsets from distinct lineages were activated with distinct stimuli to induce biologically relevant responses: T cell subsets were stimulated by cross-linking T cell and costimulatory receptors (anti-CD3/CD28 Dynabeads)^{27–29}; B cell subsets were stimulated with antihuman immunoglobulin G (IgG)/IgM and human interleukin-4 (IL-4) (refs.^{30–32}); monocytes were stimulated with lipopolysaccharide⁹; and NK cells were stimulated with IL-2-, CD2- and cytotoxic and regulatory T cell molecule (natural cytotoxicity triggering receptor 1)-coated beads³³. The duration of stimuli exposure was chosen according to the corresponding literature; activation status was confirmed by inspecting surface expression of CD69 (Supplementary Fig. 7).

Overall, stimulation drives dramatic changes in the chromatin landscapes of B and T cells. In contrast, we saw only limited effects in innate lineage cells (Supplementary Fig. 5a,b). On further inspection of the monocyte dataset, even though differentially expressed genes replicated the results from Alasoo et al.¹⁰, we did not observe a robust stimulation response at the chromatin level or changes in CD69 surface expression (Supplementary Figs. 6b,c and 7). Therefore, we do not discuss the stimulated monocytes further.

Stimulation was a major driver of sample clustering of B and T cells (Fig. 3a). The primary axes of variation in chromatin accessibility

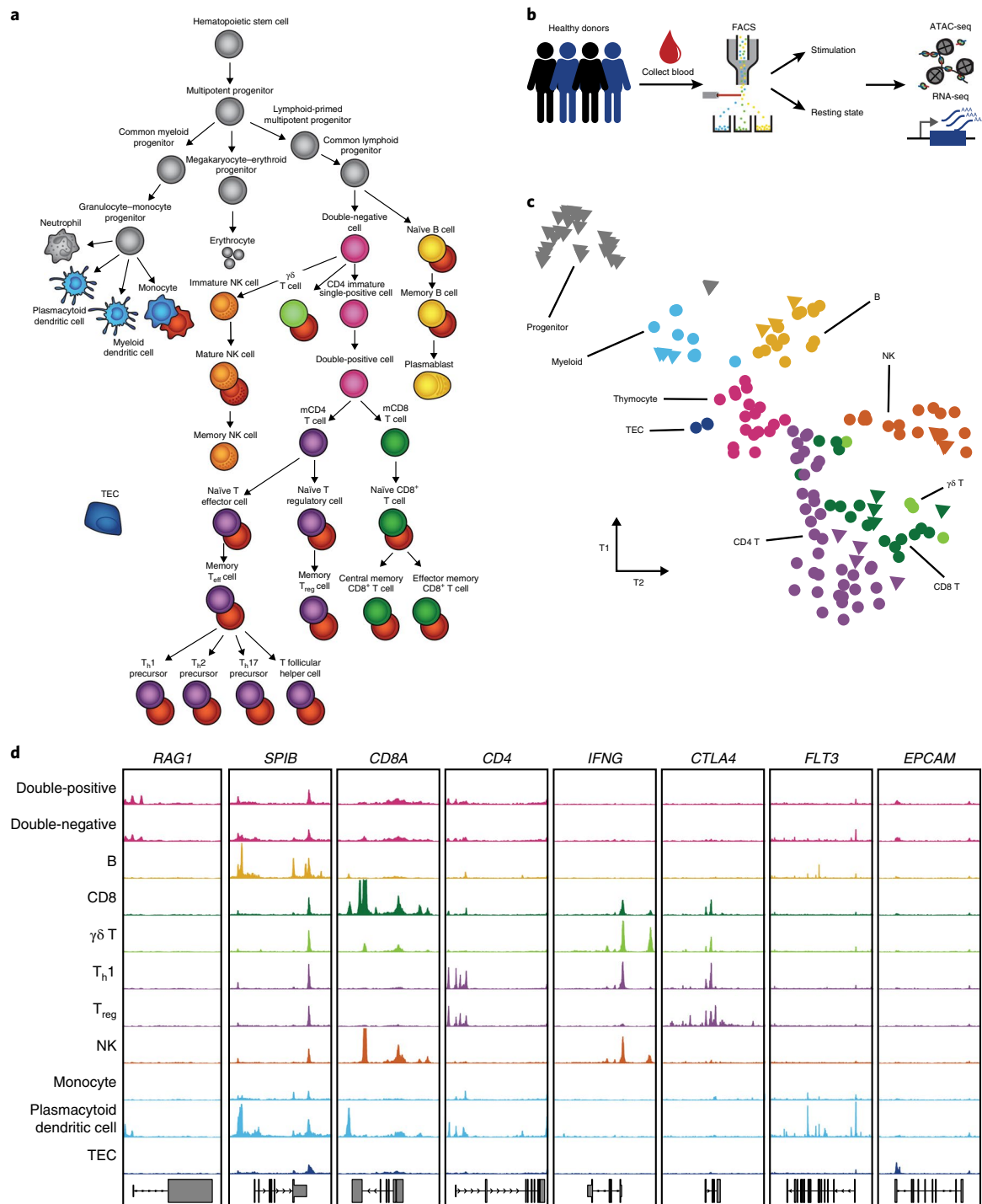


Fig. 1 | Study workflow and *t*-distributed stochastic neighbor embedding of ATAC-seq data. **a**, Illustration of isolated cell types, which include cell types that were previously published (gray), as well as resting (colored) and stimulated (red) immune cells obtained from this study. **b**, Schematic of the sample processing pipeline. Immune cells from up to four healthy donors were sorted by flow cytometry, activated and subjected to ATAC-seq and RNA-seq. **c**, Exploratory *t*-distributed stochastic neighbor embedding of ATAC-seq chromatin accessibility from all cell types in a resting state. Each sample is colored by broad cell lineage. Samples for each cell type from different donors are plotted separately (counts can be found in Supplementary Table 1). The triangles represent previously published data¹⁹ and the circles represent data generated in this study. **d**, Representative ATAC-seq profiles (y axis, 0–400 RPKM) at several cell-type-specific genes (see Methods).

were associated with both stimulation and cell type. Moreover, stimulated samples moved in a similar direction, suggesting an underlying shared chromatin response to stimulation. Furthermore, many similar pathways were enriched for significant stimulation-associated genes among distinct subsets (Supplementary Fig. 8 and Supplementary Table 1).

To quantify these observations, we used a random effects model to estimate the proportion of biological variance of chromatin accessibility explained by stimulation condition, lineage (CD4⁺, CD8⁺ and B) and cell subset (for example, naïve, memory and T helper cells; Methods). We found that stimulation, regardless of lineage or cell type, accounted for roughly a quarter of the explained

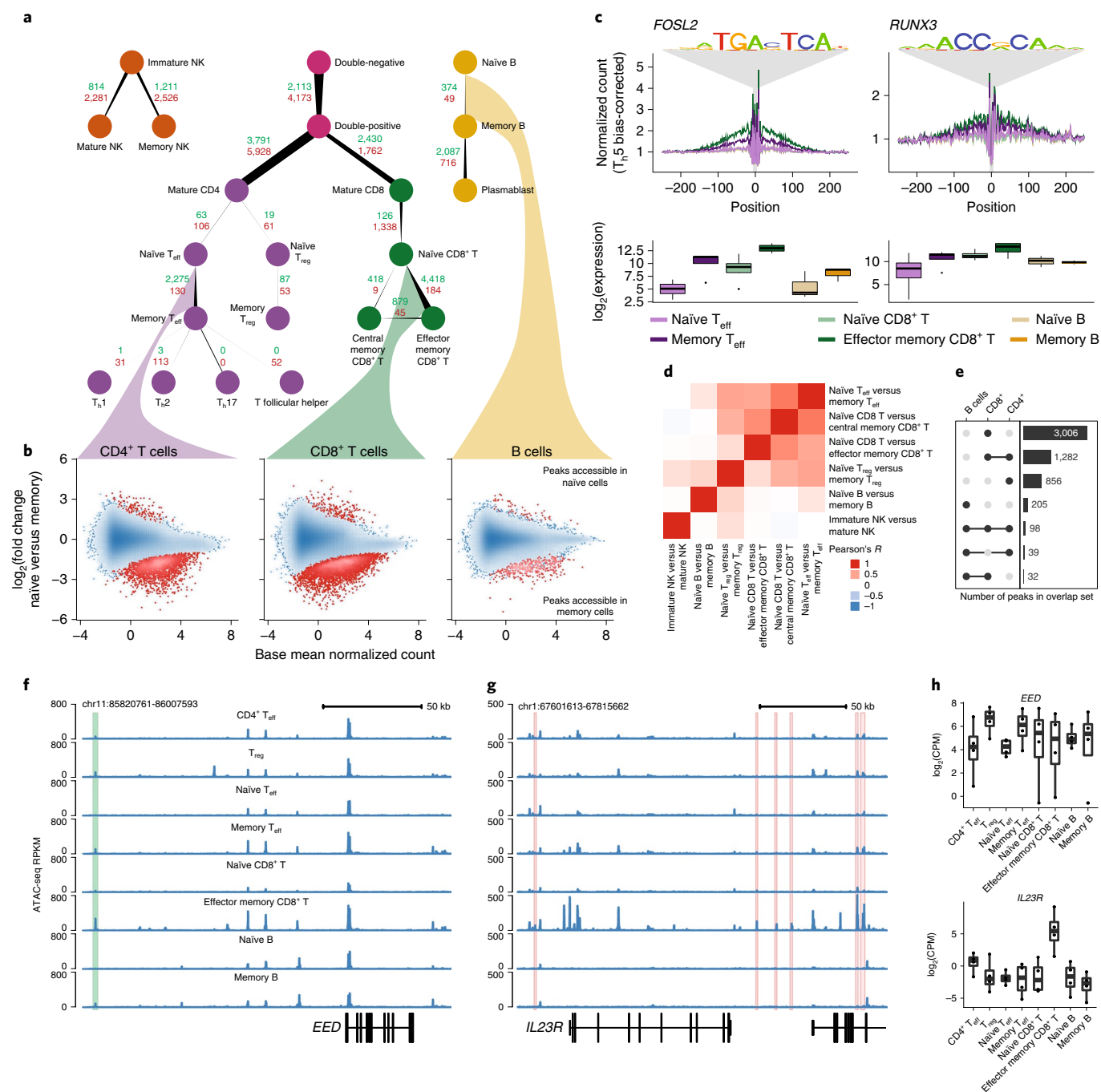


Fig. 2 | Identification of accessible regions associated with memory. **a**, Number of differentially accessible regions when comparing cell subtypes to their progenitors. The count of regions that gain versus lose accessibility are labeled green and red, respectively. The edge starting and ending widths are proportional to the numbers of peaks losing and gaining accessibility. **b**, Example M (log ratio) and A (mean average) plots comparing accessibility during the transition from naïve to memory states. Point density is shown as the blue shading. The 0.1% of points in the least densely populated regions of the plot are shown as separate points. **c**, Transcription factor footprints showing genome-wide aggregate accessibility at PWM-predicted binding sites stratified by cell subset and with the distribution of normalized RNA expression of corresponding genes. **d**, Heatmap displaying Pearson's *R* correlation between log₂(fold change) estimates of memory-associated chromatin changes between cell subsets. **e**, UpSet⁵¹ plot of the number of shared or unique regions that gain accessibility in memory formation in T and B cell lineages. **f**, ATAC-seq profile highlighting a region that increases in accessibility on transition to memory, which is shared among multiple cell types. **g**, ATAC-seq profile highlighting a region associated with effector memory CD8⁺ T cells that contains a GWAS variant linked with either Crohn's disease, ankylosing spondylitis or primary biliary cirrhosis. **h**, Box plot (see Methods) of the gene expression of the genes highlighted in **f** and **g**. All comparisons were performed on cells in a resting state; the number of samples used is listed in Supplementary Table 1.

chromatin variation (Fig. 3b). In fact, the chromatin differences due to stimulation were nearly as large as differences between cell lineages (25 versus 32%, respectively). Additionally, lineage-dependent stimulation changes explained a significantly greater

amount of chromatin variation than cell subset-specific stimulation. In summary, broadly shared stimulation and lineage-specific stimulation effects drove a large proportion of observed chromatin variation.

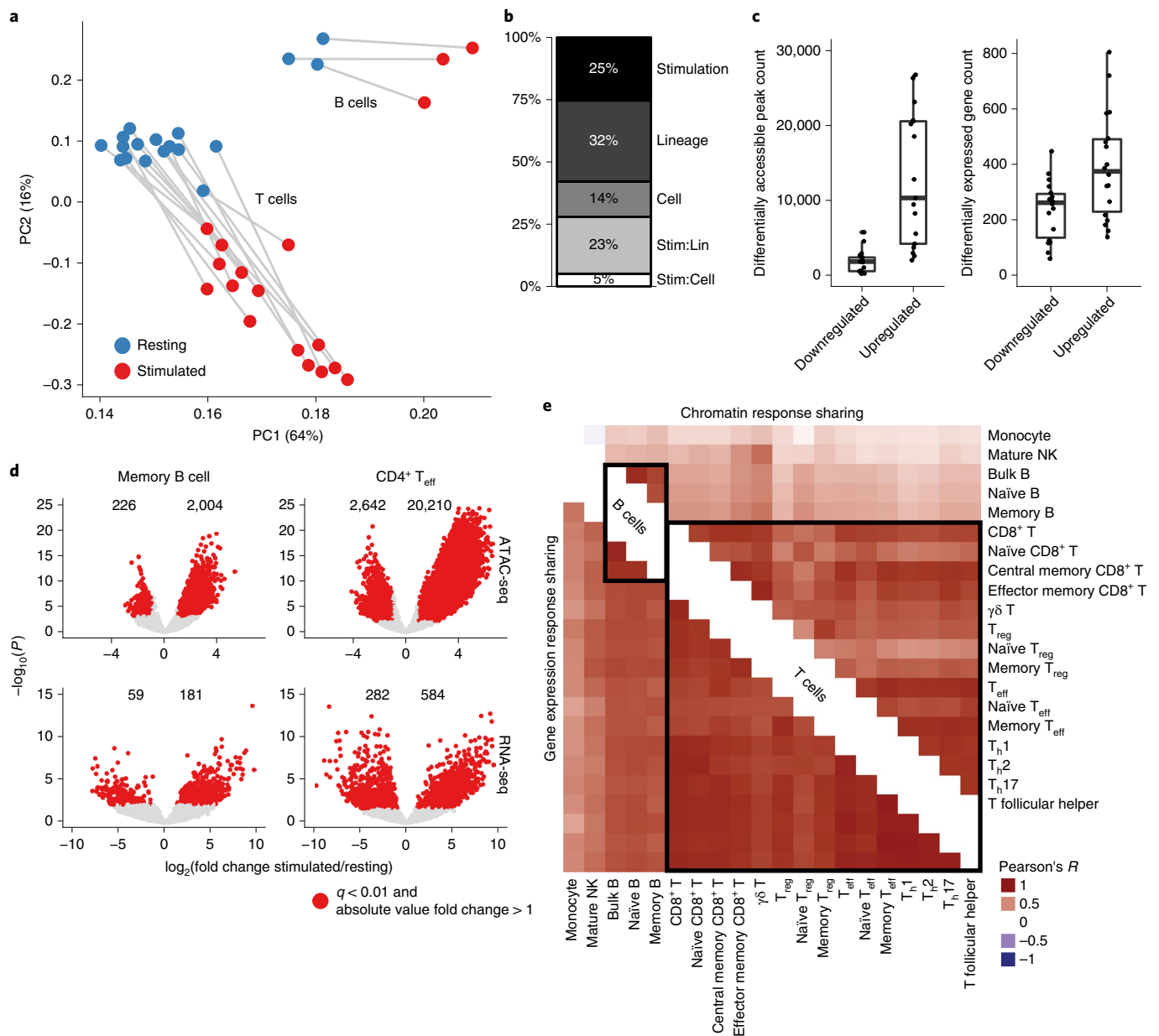


Fig. 3 | Stimulation induces large-scale changes in chromatin and gene expression in B and T cells. **a**, PCA of ATAC-seq read counts of B and T cell subsets (excluding plasmablasts), which were merged from multiple donors. Analysis is based on the top 100,000 most variable peaks. **b**, Explained proportion of variation in chromatin accessibility of the samples in **a** with at least three biological replicates, explained by biological factors of interest (see Methods). The interaction effect for lineage is labeled Stim:Lin and the interaction effect for cell type is labeled Stim:Cell. **c**, Counts of significant differentially accessible chromatin regions (left) and expressed genes (right) identified for B and T cells during stimulation (see Methods). Naïve T regulatory (T_{reg}) cells were excluded due to a lack of power because we had too few biological samples passing quality control. **d**, Volcano plots showing the stimulation effects for ATAC-seq (top) and RNA-seq (bottom) for memory B (left) and CD4⁺ effector T (T_{eff}) (right) cells. **e**, Pearson's *R* correlation between samples from stimulation response chromatin (top right triangle) and gene expression (bottom left triangle) effects, at sites or genes with a significant stimulation response in at least one of the two cell types in the comparison. All estimates are from at least three biological replicates, except for the naïve T_{reg} cells, which had two. The counts of the number of samples included and overlapping significant stimulation-associated peaks between cell subsets can be found in Supplementary Table 1.

One major effect of stimulation was a marked increase in the number of accessible sites and in the widespread upregulation of gene expression (Fig. 3c). Specifically, we found 30,224 additional peaks in stimulated cell types compared to resting state (Supplementary Fig. 5c). Testing for differential accessibility, we found, on average, that 12,119 peaks were significantly more accessible, versus 1,722 peaks that were significantly less accessible following stimulation (Fig. 3c, left panel and Supplementary

Dataset 3). We observed a similar pattern in gene expression where, per sample, an average of 394 genes were upregulated compared to 237 downregulated genes in stimulated cell types relative to their resting cell state (Fig. 3c, right panel and Supplementary Dataset 4).

For example, stimulation of memory B cells leads to considerable increases of accessibility and expression. At the same time, only 226 peaks become less accessible and 59 genes are downregulated

following stimulation. We found a similar trend within subsets of the T cell lineage (Fig. 3d).

Finally, given that both B cell and T cell subsets have highly distinct functions during an immune response, we were interested in quantifying the strength of the shared effects of stimulation on chromatin remodeling. Therefore, we computed the Pearson's R correlation of effects estimated from stimulation-induced changes in chromatin accessibility and gene expression between each pair of cell types as a summary statistic of the shared effect of stimulation (Fig. 3e).

We observed large proportions of shared stimulation-induced, chromatin-accessible regions between CD4⁺, CD8⁺ and $\gamma\delta$ T cells (mean $R=0.74$) on activation. Similarly, we observed strong sharing among B cell subsets (mean $R=0.82$). Furthermore, despite the divergent mechanisms of activation in B and T cells, we identified a significant level of sharing globally between stimulation response in B and T cells (mean $R=0.37$), indicating that some stimulation-induced regulatory networks are utilized by both B and T cells. However, while stimulation induces both unique and shared chromatin responses, stimulation-induced transcriptional signatures are broadly shared among cell types (mean $R=0.77$). We further characterize the transcription factors driving stimulation-induced chromatin effects and their connection to gene expression in the Supplementary Note.

Context-specific allelic imbalance. In addition to identifying stimulation-associated chromatin regions, we were interested in characterizing genetic variants that alter context-specific chromatin regulation. Due to the small number of individuals included in this study, and thus insufficient power to call chromatin accessibility quantitative trait loci, we used the observed allelic imbalance of ATAC-seq reads that map to heterozygous SNPs to identify significant sites of allele-specific chromatin accessibility (ASC). The hypothesis is that a heterozygous variant may cause local, allele-specific changes in chromatin accessibility, for example, by disrupting local transcription factor binding. Such events result in an imbalance in the number of ATAC-seq reads overlapping each allele^{34–38}. After read filtering to account for mapping biases³⁹, we computed binomial test P values and identified 607 significant ASC sites, on average, per sample, and a total of 10,780 sites overall ($q < 0.1$; see Methods and Supplementary Table 1).

Because we collected many cell samples from each donor, we could test for allelic imbalance of chromatin accessibility at an individual heterozygous site across cell- and condition-specific contexts. For instance, we observed a heterozygous variant, rs3795671, that resulted in increased chromatin accessibility at the reference allele across resting and stimulated samples (Fig. 4a). Other variants exhibited allelic imbalance in a subset of cell type states; these include rs7011799, rs12091715, rs1250567 and rs1445033, which are associated with chromatin accessibility within resting, stimulated, T and B lineage contexts, respectively.

Next, we leveraged these data to verify transcription factors that regulate chromatin in specific contexts and thus drive context-specific allelic imbalance. As described in the Supplementary Note, motif enrichment analysis (Supplementary Fig. 5d) suggested that B cell-activating transcription factor (B-ATF)—or perhaps another transcription factor from the AP-1 family, which can have similar position weight matrices (PWMs)—among others, is an important regulator of chromatin in stimulated cells²⁶. Therefore, we hypothesized that sites that affect B-ATF binding would result in ASC within stimulated samples. As a proxy for true B-ATF binding, for each heterozygous site within a B-ATF binding motif, we computed the relative binding affinity for the reference and the alternative allele using the B-ATF PWM. On stimulation, alleles that were predicted to increase B-ATF binding affinity were associated with increased accessibility. However, there was no such effect in resting cells,

indicating that B-ATF does not impact chromatin accessibility in the resting state (Fig. 4b). We observed a similar preferential binding effect for other stimulation-associated transcription factors, including transcription factor jun-B, Fos-related antigen 1 and transcription regulator protein BACH1 (Supplementary Fig. 9a). Thus, the PWMs of these factors can predict sequence-dependent changes of stimulation-specific effects on chromatin accessibility. However, because of the correlation between PWMs of distinct transcription factors, further study is required to link these signals definitively to specific transcription factors.

Intrigued by the stimulation-specific effect of the B-ATF-associated PWM, we wanted to leverage our ASCs to determine the prevalence of context-specific chromatin regulation. We propose three possible models of chromatin effects at a significant ASC site, in pairs of cell types or conditions (Fig. 4c, from left to right). The variant can: (1) differentially affect chromatin in cell type A, while the region is inaccessible in cell type B; (2) differentially affect chromatin in cell type A, but not in cell type B, even though the region is accessible therein; (3) differentially affect chromatin in both cell types. The relative fractions of case 2 versus case 3 were estimated using a method that accounts for incomplete power in each statistical test⁴⁰.

We quantified the proportion of ASCs that fit each possible model and observed that most ASCs have shared effects on chromatin regulation (Methods). To further investigate changes in the prevalence of shared regulation across differences in cell state, we varied whether the two compared samples were of the same lineage and condition. For the purpose of this analysis, we grouped all 'stimulated' samples.

Notably, most effects on allelic imbalance were shared regardless of lineage or condition (Fig. 4d). In contrast, the proportion of accessible sites covaried more strongly with differences in lineage and condition between the two samples. These observations suggest that changes in cellular function due to chromatin remodeling occur primarily through changes in chromatin accessibility, rather than regulation of already accessible chromatin. Moreover, these trends held when the analysis was performed in the other donors (Supplementary Fig. 9b,c). The B-ATF analysis in Fig. 4b indicates that at least some sites containing B-ATF motifs are probably differentially regulated on stimulation; however, this scenario represents a small minority of all ASC sites, which corroborates findings from previous studies on chromatin accessibility quantitative trait loci⁴¹.

GWAS enrichment in immune-specific accessible regions.

Understanding the molecular mechanisms behind autoimmune disease risk variants requires the identification of disease-relevant cell types and states. With chromatin accessibility information from a large number of resting and activated immune cell types, we can identify cell types and conditions enriched for variants associated with autoimmune disease. For example, the inclusion of thymocytes and progenitor cells allow us to examine the possibility that autoimmunity risk variants affect enhancers that are selectively accessible during early differentiation.

Using publicly available summary statistics for nine autoimmune disorders and four nonimmune traits (as controls), we identified trait-relevant functional annotations using the partitioning heritability functionality of linkage disequilibrium (LD) Score regression². This allowed us to compute the proportion of heritability explained by SNPs in open chromatin for a particular cell type. This quantity, divided by the overall proportion of open chromatin SNPs in that cell type, is referred to as the enrichment of heritability (Supplementary Table 1).

We observed greater enrichment of heritability in differentiated immune cells compared to progenitor cells and nonimmune tissues for most autoimmune traits (Fig. 5a and Supplementary Fig. 5a,b). Specifically for rheumatoid arthritis we saw about tenfold

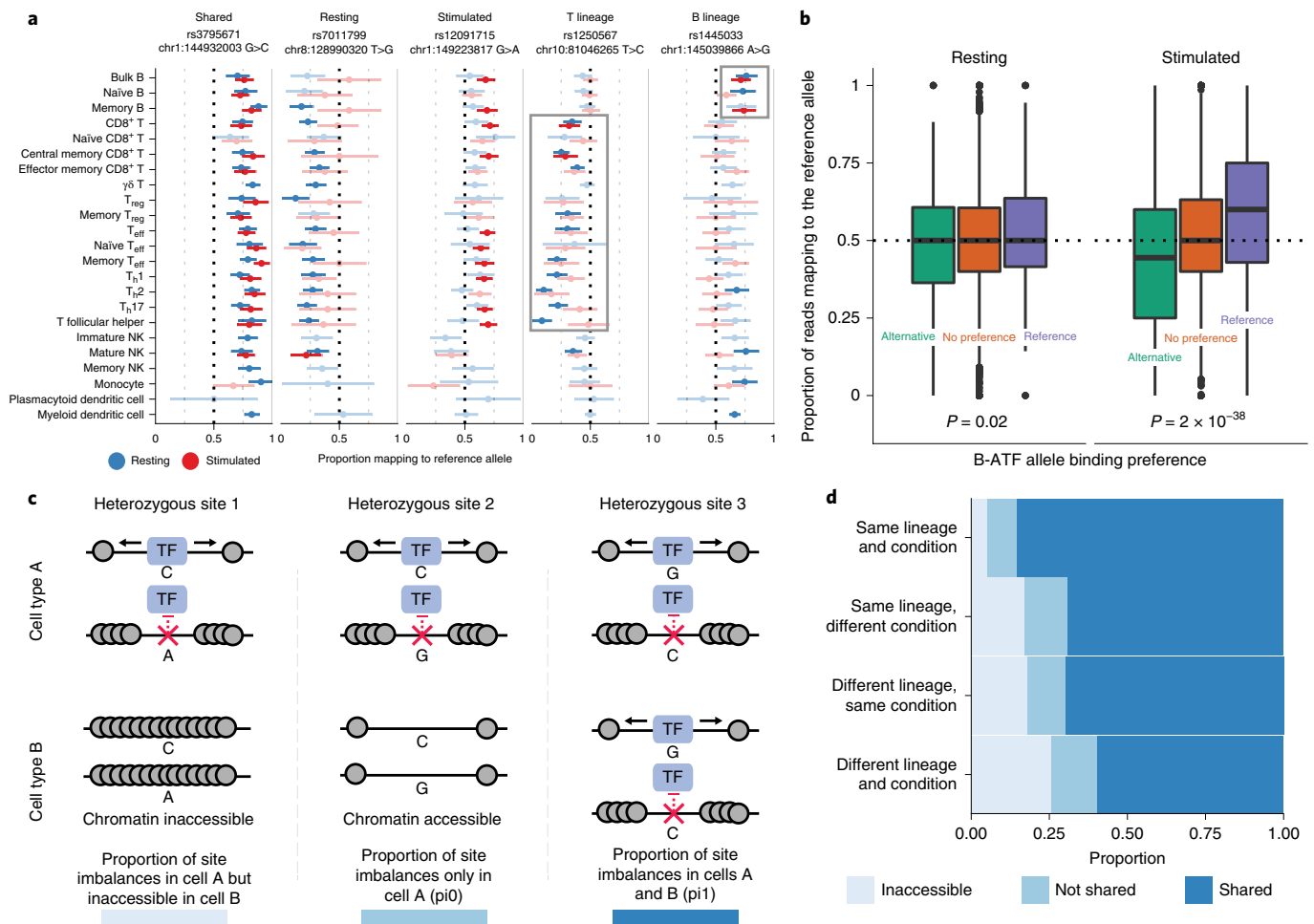


Fig. 4 | Observed allelic imbalance in chromatin accessibility data. **a**, Examples of allele-specific chromatin accessibility imbalance shared across various groups. For each heterozygous site, we display the proportion of reads mapping to the reference allele (x axis) for cell samples (y axis). The error bars represent the 95% confidence intervals computed from read depth. Samples without significant imbalance are lightly shaded. We excluded samples with fewer than four reads at the specific variant from the visualization. **b**, Heterozygous sites were grouped into three bins based on the PWM-predicted B-ATF binding affinity: preference for the alternative allele; no preference; preference for the reference allele. The y axis represents the aggregate proportion of reads mapping to the reference allele for these groups in T_{H1} precursor cells under resting (left) and stimulated (right) conditions. Sites with fewer than four reads were excluded. **c**, Scenarios of allele-specific chromatin accessibility imbalance in two different cell types or conditions for the same donor. **d**, Proportion plot displaying the estimated average proportions for each case from **c**, stratified according to whether the two samples were of the same lineage and condition. Innate cells were excluded from this analysis. All plots are for donor 1, who had the highest sequencing depth, although similar trends were found in the other donors (Supplementary Fig. 9b,c). The read counts for **a** and sample sizes for **b** and **d** can be found in Supplementary Table 1.

enrichment of heritability in open chromatin from control tissues and progenitors compared to the genome-wide background (Fig. 5a), and a median 23-fold enrichment in the open chromatin of adult immune cell types. Heritability enrichment in nonimmune tissues compared to the genome-wide background is probably due to the fact that many open chromatin regions are shared among diverse cell types. Thus, many of the SNPs that affect disease risk through immune cell functions are also located in open chromatin in many other tissues⁴².

Notably, heritability enrichment was particularly strong in stimulated immune cells compared to their resting counterparts (Fig. 5b). This signal was spread across diverse cell types, including both B cell and T cell lineages, and did not implicate particular immune subsets as drivers of rheumatoid arthritis. We wondered whether this relatively diffuse signal arises because multiple cell types play causal roles in rheumatoid arthritis, or simply because the broad sharing of stimulation peaks makes it difficult to identify a critical cell type.

To investigate this further, we grouped the open chromatin peaks into 11 disjoint clusters based on their profiles of accessibility across cell types and conditions (Methods and Supplementary Fig. 10c). For example, we defined a cluster of peaks that are open only in stimulated B cells and a cluster of peaks that are open only in stimulated T cells. We used these peak groupings to test which clusters are enriched for autoimmune trait heritability (Fig. 5c).

Overall, we observed strong enrichment of heritability in accessible regions from multiple peak groups, especially among the stimulation-related peaks. No single peak group could explain the entirety of the signal. Since these groups are disjoint, this observation implies that multiple separate immune components contribute to heritability. In the case of rheumatoid arthritis, we identified enriched heritability in stimulation peaks specific to B lineage cells and in stimulation regions specific to T lineage cells, thus implicating a role for both stimulated B and T cells. Previous studies have separately identified B^{19,43} and T cells^{1,4} in driving the development of rheumatoid arthritis, although our analysis would suggest that

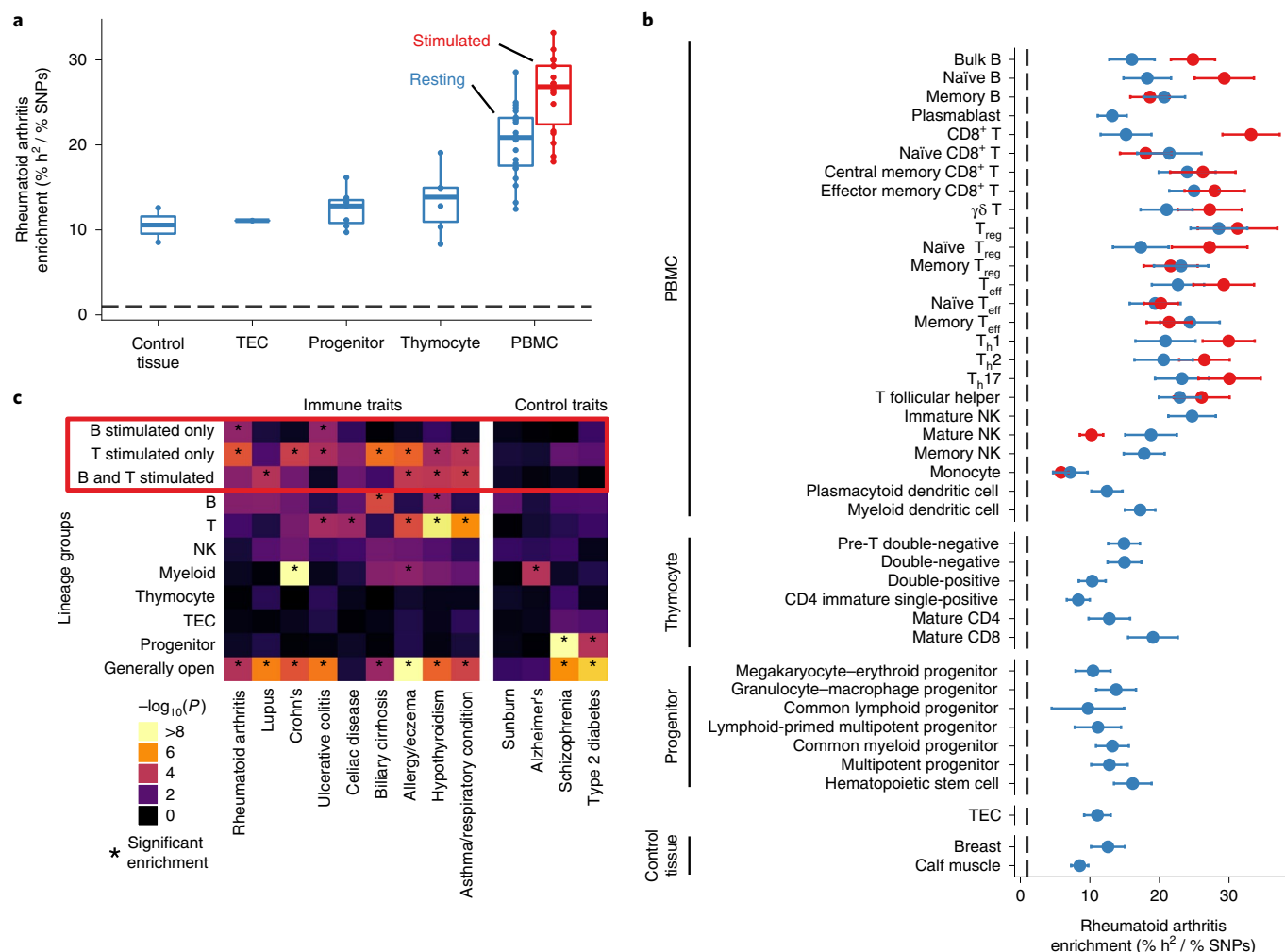


Fig. 5 | GWAS analysis of accessible regions. **a**, Rheumatoid arthritis heritability enrichment is aggregated by differentiation and condition. Stimulated innate cells were excluded from this visualization. The dashed line represents a baseline proportion of disease heritability across all SNPs. **b**, Enrichment of rheumatoid arthritis heritability (x axis) in open chromatin regions for resting (blue) and stimulated (red) samples (y axis). The error bars indicate ± 1 s.d. The dashed line represents a baseline proportion of disease heritability across all SNPs. **c**, We grouped peaks into disjoint clusters based on their patterns of accessibility across cell types (x axis). Then, we used the partitioning heritability functionality of LD Score regression to estimate enrichments of trait signal (x axis) in these peak clusters (y axis). We highlighted groups of peaks related to stimulation with a red box; the asterisks indicate significant enrichment of trait heritability (Bonferroni-adjusted $P < 0.05$). The sample sizes for **a–c** can be found in Supplementary Table 1.

both contribute to autoimmunity. In addition to signals from cell type-specific clusters, all traits had significant enrichment within loci that were broadly accessible, highlighting the contribution of broadly open ‘housekeeping’ peaks to heritability.

Taken together, these results suggest that stimulated cells from both B and T lineages probably contribute to autoimmunity. Furthermore, it remains difficult to implicate more narrowly defined subsets through this type of analysis due to the extensive sharing of open chromatin among closely related subsets.

Stimulation-specific data increase GWAS and eQTL overlap.

One important approach for linking noncoding GWAS hits to the genes they regulate is through eQTL mapping. However, only a small proportion of significant GWAS sites have been successfully linked to an eQTL. One hypothesis for the limited overlap is that many eQTLs may be context-specific and thus remain unidentified if not all of the relevant cell types or conditions have been studied¹⁴. Since we found a strong signal of autoimmune trait risk variants located within stimulation-specific chromatin accessibility peaks, we sought to investigate whether these variants would have been

identified as candidate regulatory variants in a standard tissue-based eQTL study. We present results primarily from rheumatoid arthritis because the heritability of this disorder was highly enriched in the stimulation-specific accessible regions in our previous analysis.

For this analysis, we partitioned the set of allelic imbalance sites into two groups: ASC sites that were identified in resting samples; and ASC sites that were only identified in stimulated samples (either B or T cells; nominal $P < 0.10$). In this analysis, sites that were present in both resting and stimulated cells were included in the resting set, since those could be identified even without using stimulated cell data. Since variants that affect chromatin accessibility are strongly associated with regulation of gene expression³⁴, the former set of ASCs probably contains sites that regulate gene expression in the resting cell state, while the latter contains sites associated with stimulation-specific gene regulation.

Both sets of SNPs exhibited highly significant enrichment of rheumatoid arthritis GWAS signal relative to control SNPs ($P = 2 \times 10^{-19}$ (resting) and $P = 3 \times 10^{-14}$ (stimulation-only); Fig. 6a). However, the stimulation-specific ASCs would not have been identified in the resting samples. Moreover, we compared these two sets

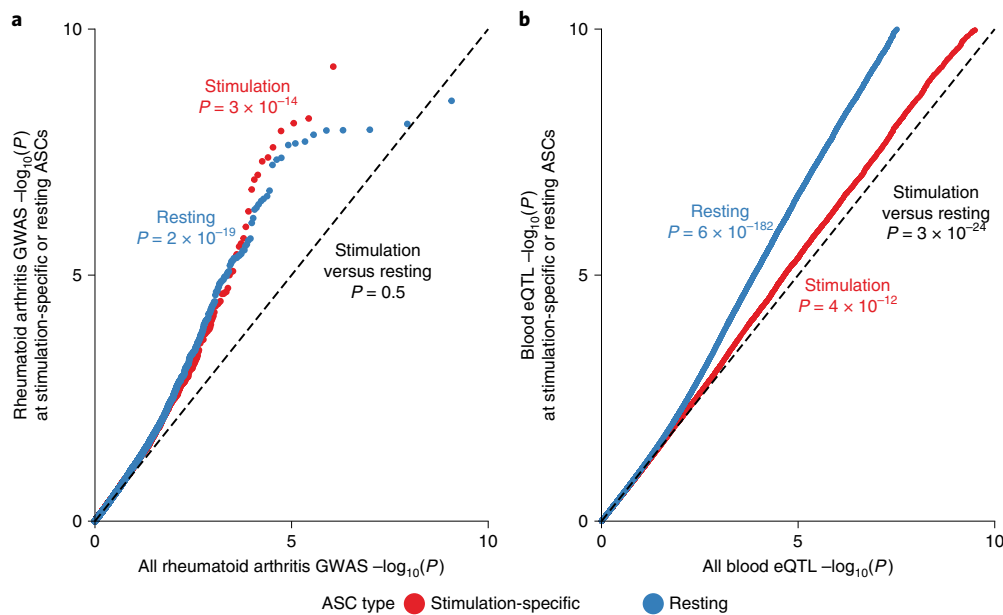


Fig. 6 | GWAS and eQTL enrichment in sites of allele-specific chromatin. **a**, Comparison of rheumatoid arthritis GWAS enrichment within the set of SNPs that regulate chromatin accessibility, in either B or T cells, under stimulation (red) or resting (blue) conditions. **b**, Comparison of eQTL signal in the same two sets of variants from **a**, using eQTL data from GTEx v.7. For both plots, the x axis reflects an empirical distribution of P values. Sample sizes can be found in Supplementary Table 1. We computed P values with a two-sided Mann–Whitney U -test.

to all variants for which an ASC P value was computed and similar trends were observed (Supplementary Fig. 11a). Thus, stimulation-specific chromatin is as important, in terms of disease risk enrichment, as resting-specific chromatin from immune cells.

Thus far, there have been many studies of blood eQTLs (peripheral blood mononuclear cells (PBMCs)) encompassing many thousands of samples⁴⁵. However, since the proportion of stimulated cells in bulk tissues is relatively low, we hypothesized that sites that affect stimulation-specific chromatin accessibility may not be detected as eQTLs using whole blood or resting immune cells. To test this hypothesis, we determined the enrichment of blood eQTL signal from the Genotype-Tissue Expression (GTEx) Project in the two previously described sets of resting and stimulation-specific ASC sites. We observed a strong enrichment ($P = 3 \times 10^{-24}$) of blood eQTL signal within the resting state-specific set of ASC variants compared to the stimulation-specific set (Fig. 6b). Furthermore, a similar trend was observed when using eQTLs from naïve T cells (Supplementary Fig. 11b) (ref. 7). These observations indicate a clear need for large-scale eQTL mapping in stimulated immune cells and argue that the low overlap of autoimmune GWAS and eQTL data⁸ is at least partly driven by the current lack of such data.

These observations suggest that the inclusion of data from stimulated cells could help fine-map previously unexplained causal mutations. To identify such examples, we intersected a database of fine-mapped candidate causal GWAS SNPs¹ with a set of stimulation-specific allelic imbalance heterozygous SNPs and PWM disruption scores for transcription factors (Supplementary Dataset 5).

Using these data, we identified a T cell lineage-specific stimulation peak within an intergenic region upstream of the *TNFAIP3* locus (encoding the protein A20). Moreover, this region contains several variants that are included in a credible set of regions identified for rheumatoid arthritis and ulcerative colitis. For rheumatoid arthritis, only rs6927172 falls within a stimulation-specific chromatin-accessible peak (Fig. 7a). For ulcerative colitis, in addition to rs6927172, three additional variants fall within another nearby stimulation-responsive peak, yet this second peak does not demonstrate as strong a response as the first peak (Supplementary Fig. 13a).

Notably, rs6927172 was associated with altered chromatin accessibility in stimulated CD4⁺ T cells across multiple donors, suggesting a potential role of the SNP in regulating chromatin remodeling (Fig. 7b).

Indeed, the cytosine to guanine mutation leads to a large change in the PWM-predicted binding affinity of the p50 subunit of NFκB1 (Fig. 7c and Supplementary Fig. 13b; see Supplementary Fig. 13c for the expression levels). To validate this observation, we performed chromatin immunoprecipitation sequencing (ChIP-seq) for the p65 and p50 subunits of NFκB1 from stimulated CD4⁺ T cells isolated from two healthy donors who are heterozygous for rs6927172. We observed an increased count of p50 ChIP-seq reads that mapped to the region containing our SNP of interest in one of the two donors. As predicted, we detected significant allelic imbalance for p50 in the same donor (Fig. 7d).

Since NFκB1 has been shown to regulate *TNFAIP3* expression^{46,47}, this result suggests that rs6927172 may contribute to the pathology of autoimmune diseases by disrupting the binding of NFκB1 in stimulated T cells to the *TNFAIP3* locus and therefore inhibit gene expression (Fig. 7c).

Discussion

While increasing evidence points to an important role of stimulation response in autoimmune dysregulation, little work has been done to characterize shared and cell subset-specific stimulation effects across multiple differentiation lineages. Therefore, we developed a map of stimulation-responsive chromatin accessibility and transcription in a diverse set of immune cell populations.

To study the impact of genetic variation on the chromatin landscape, we used allele-specific measurement of open chromatin to identify genotype-dependent sites (ASCs). While the majority of ASCs are shared between closely related cell types, only 60% of ASCs are shared for comparisons between lineages and between stimulated and resting cells. Most nonsharing of ASCs is due to differential accessibility between cell types/conditions, while a smaller fraction is due to differential regulation of shared open sites as exemplified by B-ATF activity in stimulated cells.

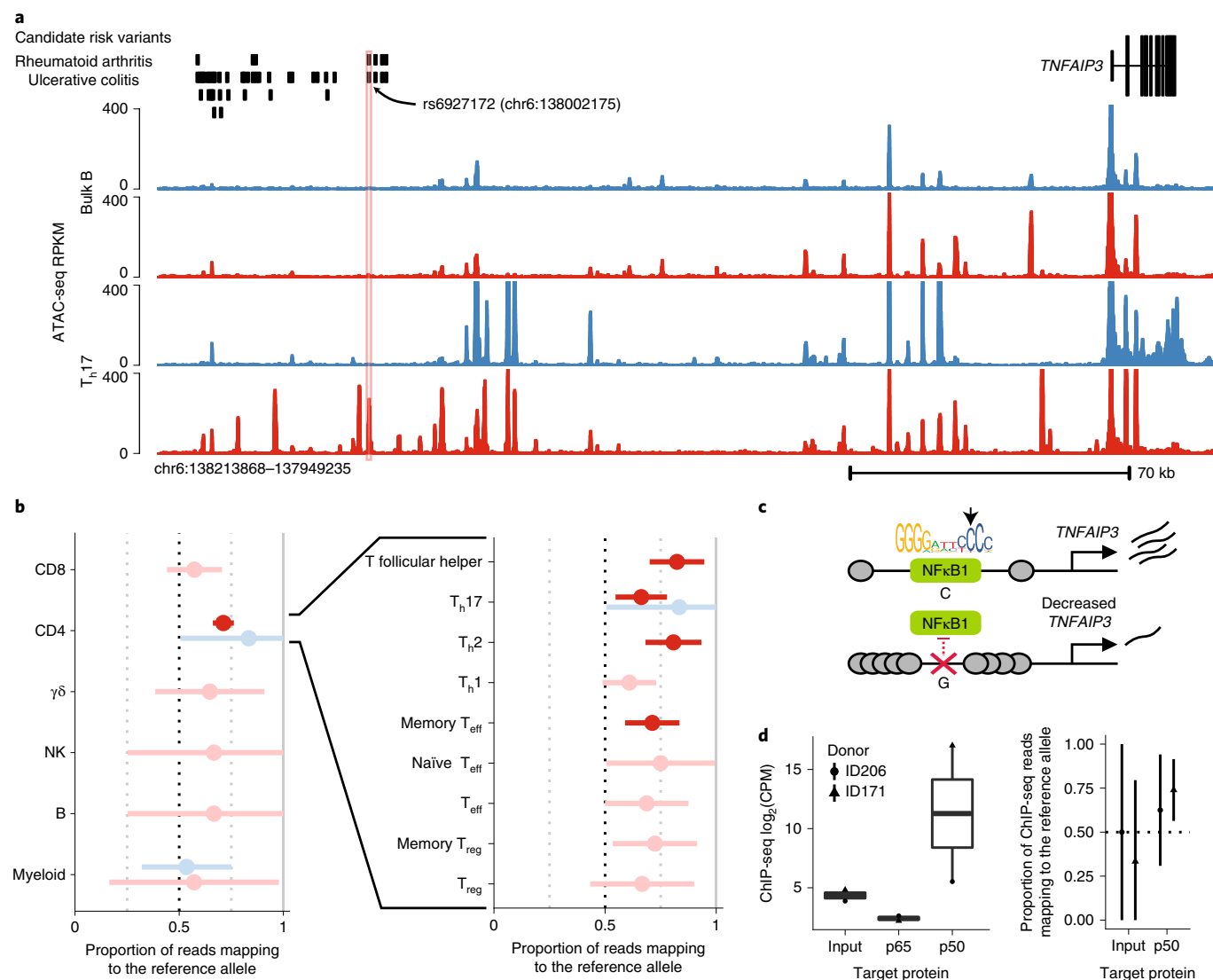


Fig. 7 | Identifying rs6927172 as a stimulation-specific chromatin regulator in a complex autoimmune GWAS region. **a**, Chromatin accessibility profile for stimulated (red) and resting (blue) bulk B (top) and T_{H17} (bottom) cells around variant rs6927172. This region contains significant GWAS signals for ulcerative colitis and rheumatoid arthritis, but the causal variant(s) have not been determined (credible set indicated). We include a trackplot with all the samples in Supplementary Fig. 12. **b**, Allele-specific ATAC-seq reads at rs6927172 in the three heterozygous donors (the fourth was not heterozygous at this site). The proportion of reads mapping to the reference allele is displayed. The error bars represent the 98% confidence intervals and were computed from read depth. Significant ($P < 0.01$) allelic imbalance associations have been colored (see Methods). The exact read counts for these sites can be found in Supplementary Table 1. **c**, A proposed negative feedback model of gene regulation linking NFkB1 to *TNFAIP3*. We included the canonical PWM for the p50 subunit of NFkB1, as downloaded from the JASPAR transcription factor motif database. The heterozygous allele disrupts the nucleotide indicated by the arrow. **d**, ChIP-seq read count for the input genomic DNA control and p50 and p65 subunits of NFkB1. Left: $n=2$ read counts, found in Supplementary Table 1. Right: allelic imbalance of ChIP-seq reads mapping to rs6927172.

Several past studies have mapped GWAS signals to cell type-specific functional elements, allowing the prediction of the cell types that may be involved in disease pathology^{1–6,48}. We observed significant autoimmune trait heritability within accessible regions of distinct stimulated cell types, suggesting contributions of multiple stimulation response components to autoimmunity. Moreover, we showed that the genetic variation associated with stimulation-specific gene regulation is significantly underrepresented in existing large-scale eQTL datasets from whole blood PBMCs. As a concrete example of this point we identified rs6927172, which was associated with $CD4^+$ T cell stimulation-specific changes in chromatin accessibility near *TNFAIP3* and affects the predicted binding of the p50 subunit of NFkB1. This region has been associated with several autoimmune phenotypes, such as variable patient responses

to anti-tumor necrosis factor treatment⁴⁹, ulcerative colitis¹⁵ and rheumatoid arthritis⁵⁰. We further propose a model by which this variant affects autoimmunity in the Supplementary Note.

Taken together, these data provide insights into the interplay of specific loci and regulatory networks involved in the human immune system. Additionally, we present a powerful platform to map genetic variants to cell- and context-specific functional regions genome-wide, and therefore, to their context-specific effects on disease phenotypes.

Online content

Any methods, additional references, Nature Research reporting summaries, source data, statements of code and data availability and associated accession codes are available at <https://doi.org/10.1038/s41588-019-0505-9>.

Received: 30 January 2019; Accepted: 27 August 2019;
Published online: 30 September 2019

References

- Farh, K. K. et al. Genetic and epigenetic fine mapping of causal autoimmune disease variants. *Nature* **518**, 337–343 (2015).
- Finucane, H. K. et al. Partitioning heritability by functional annotation using genome-wide association summary statistics. *Nat. Genet.* **47**, 1228–1235 (2015).
- Pickrell, J. K. Joint analysis of functional genomic data and genome-wide association studies of 18 human traits. *Am. J. Hum. Genet.* **94**, 559–573 (2014).
- Hu, X. et al. Integrating autoimmune risk loci with gene-expression data identifies specific pathogenic immune cell subsets. *Am. J. Hum. Genet.* **89**, 496–506 (2011).
- Maurano, M. T. et al. Systematic localization of common disease-associated variation in regulatory DNA. *Science* **337**, 1190–1195 (2012).
- Trynka, G. et al. Chromatin marks identify critical cell types for fine mapping complex trait variants. *Nat. Genet.* **45**, 124–130 (2013).
- Chen, L. et al. Genetic drivers of epigenetic and transcriptional variation in human immune cells. *Cell* **167**, 1398–1414.e24 (2016).
- Chun, S. et al. Limited statistical evidence for shared genetic effects of eQTLs and autoimmune-disease-associated loci in three major immune-cell types. *Nat. Genet.* **49**, 600–605 (2017).
- Kim-Hellmuth, S. et al. Genetic regulatory effects modified by immune activation contribute to autoimmune disease associations. *Nat. Commun.* **8**, 266 (2017).
- Alasoo, K. et al. Shared genetic effects on chromatin and gene expression indicate a role for enhancer priming in immune response. *Nat. Genet.* **50**, 424–431 (2018).
- Fairfax, B. P. et al. Innate immune activity conditions the effect of regulatory variants upon monocyte gene expression. *Science* **343**, 1246949 (2014).
- Lee, M. N. et al. Common genetic variants modulate pathogen-sensing responses in human dendritic cells. *Science* **343**, 1246980 (2014).
- Ye, C. J. et al. Intersection of population variation and autoimmunity genetics in human T cell activation. *Science* **345**, 1254665 (2014).
- Simeonov, D. R. et al. Discovery of stimulation-responsive immune enhancers with CRISPR activation. *Nature* **549**, 111–115 (2017).
- Huang, H. et al. Fine-mapping inflammatory bowel disease loci to single-variant resolution. *Nature* **547**, 173–178 (2017).
- Onengut-Gumuscu, S. et al. Fine mapping of type 1 diabetes susceptibility loci and evidence for colocalization of causal variants with lymphoid gene enhancers. *Nat. Genet.* **47**, 381–386 (2015).
- de Lange, K. M. et al. Genome-wide association study implicates immune activation of multiple integrin genes in inflammatory bowel disease. *Nat. Genet.* **49**, 256–261 (2017).
- Buenrostro, J. D., Giresi, P. G., Zaba, L. C., Chang, H. Y. & Greenleaf, W. J. Transposition of native chromatin for fast and sensitive epigenomic profiling of open chromatin, DNA-binding proteins and nucleosome position. *Nat. Methods* **10**, 1213–1218 (2013).
- Corces, M. R. et al. Lineage-specific and single-cell chromatin accessibility charts human hematopoiesis and leukemia evolution. *Nat. Genet.* **48**, 1193–1203 (2016).
- Moskowitz, D. M. et al. Epigenomics of human CD8 T cell differentiation and aging. *Sci. Immunol.* **2**, eaag0192 (2017).
- van der Veecken, J. et al. Memory of inflammation in regulatory T cells. *Cell* **166**, 977–990 (2016).
- He, B. et al. CD8⁺ T cells utilize highly dynamic enhancer repertoires and regulatory circuitry in response to infections. *Immunity* **45**, 1341–1354 (2016).
- Yu, B. et al. Epigenetic landscapes reveal transcription factors that regulate CD8⁺ T cell differentiation. *Nat. Immunol.* **18**, 573–582 (2017).
- Leslie, R., O'Donnell, C. J. & Johnson, A. D. GRASP: analysis of genotype-phenotype results from 1390 genome-wide association studies and corresponding open access database. *Bioinformatics* **30**, i185–i194 (2014).
- Ostuni, R. et al. Latent enhancers activated by stimulation in differentiated cells. *Cell* **152**, 157–171 (2013).
- Gate, R. E. et al. Genetic determinants of co-accessible chromatin regions in activated T cells across humans. *Nat. Genet.* **50**, 1140–1150 (2018).
- Hess, K. et al. Kinetic assessment of general gene expression changes during human naive CD4⁺ T cell activation. *Int. Immunol.* **16**, 1711–1721 (2004).
- Diehn, M. et al. Genomic expression programs and the integration of the CD28 costimulatory signal in T cell activation. *Proc. Natl Acad. Sci. USA* **99**, 11796–11801 (2002).
- Trickett, A. & Kwan, Y. L. T cell stimulation and expansion using anti-CD3/CD28 beads. *J. Immunol. Methods* **275**, 251–255 (2003).
- Wortis, H. H., Teutsch, M., Higer, M., Zheng, J. & Parker, D. C. B-cell activation by crosslinking of surface IgM or ligation of CD40 involves alternative signal pathways and results in different B-cell phenotypes. *Proc. Natl Acad. Sci. USA* **92**, 3348–3352 (1995).
- Van Belle, K. et al. Comparative in vitro immune stimulation analysis of primary human B cells and B cell lines. *J. Immunol. Res.* **2016**, 5281823 (2016).
- Hodgkin, P. D., Go, N. F., Cupp, J. E. & Howard, M. Interleukin-4 enhances anti-IgM stimulation of B cells by improving cell viability and by increasing the sensitivity of B cells to the anti-IgM signal. *Cell. Immunol.* **134**, 14–30 (1991).
- Rieckmann, J. C. et al. Social network architecture of human immune cells unveiled by quantitative proteomics. *Nat. Immunol.* **18**, 583–593 (2017).
- Degner, J. F. et al. DNase I sensitivity QTLs are a major determinant of human expression variation. *Nature* **482**, 390–394 (2012).
- Kilpinen, H. et al. Coordinated effects of sequence variation on DNA binding, chromatin structure, and transcription. *Science* **342**, 744–747 (2013).
- Kasowski, M. et al. Extensive variation in chromatin states across humans. *Science* **342**, 750–752 (2013).
- McVicker, G. et al. Identification of genetic variants that affect histone modifications in human cells. *Science* **342**, 747–749 (2013).
- Neph, S. et al. An expansive human regulatory lexicon encoded in transcription factor footprints. *Nature* **489**, 83–90 (2012).
- van de Geijn, B., McVicker, G., Gilad, Y. & Pritchard, J. K. WASP: allele-specific software for robust molecular quantitative trait locus discovery. *Nat. Methods* **12**, 1061–1063 (2015).
- Stephens, M. False discovery rates: a new deal. *Biostatistics* **18**, 275–294 (2017).
- Banovich, N. E. et al. Impact of regulatory variation across human iPSCs and differentiated cells. *Genome Res.* **28**, 122–131 (2018).
- Boyle, E. A., Li, Y. I. & Pritchard, J. K. An expanded view of complex traits: from polygenic to omnigenic. *Cell* **169**, 1177–1186 (2017).
- Walsh, A. M. et al. Integrative genomic deconvolution of rheumatoid arthritis GWAS loci into gene and cell type associations. *Genome Biol.* **17**, 79 (2016).
- Ardlie, K. G. et al. Human genomics. The Genotype-Tissue Expression (GTEx) pilot analysis: multitissue gene regulation in humans. *Science* **348**, 648–660 (2015).
- Westra, H. J. et al. Systematic identification of trans eQTLs as putative drivers of known disease associations. *Nat. Genet.* **45**, 1238–1243 (2013).
- Krikos, A., Laherty, C. D. & Dixit, V. M. Transcriptional activation of the tumor necrosis factor α -inducible zinc finger protein, A20, is mediated by κ B elements. *J. Biol. Chem.* **267**, 17971–17976 (1992).
- Housley, W. J. et al. Genetic variants associated with autoimmunity drive NF κ B signaling and responses to inflammatory stimuli. *Sci. Transl. Med.* **7**, 291ra93 (2015).
- Calderon, D. et al. Inferring relevant cell types for complex traits by using single-cell gene expression. *Am. J. Hum. Genet.* **101**, 686–699 (2017).
- Bank, S. et al. Associations between functional polymorphisms in the NF κ B signaling pathway and response to anti-TNF treatment in Danish patients with inflammatory bowel disease. *Pharmacogenomics J.* **14**, 526–534 (2014).
- Thomson, W. et al. Rheumatoid arthritis association at 6q23. *Nat. Genet.* **39**, 1431–1433 (2007).
- Lex, A., Gehlenborg, N., Strobelt, H., Vuilleumot, R. & Pfister, H. UpSet: visualization of intersecting sets. *IEEE Trans. Vis. Comput. Graph.* **20**, 1983–1992 (2014).

Acknowledgements

We thank D. Yao for helping process the samples, C. J. Ye and members of the Greenleaf, Marson and Pritchard laboratories for helpful conversations and manuscript feedback. We relied on the Flow Cytometry Core at UCSF, which was supported by Diabetes Research Center grant nos. NIH P30 DK063720 and 1S10OD021822-01, and sequencing data generated by the Stanford Functional Genomics Facility on an Illumina HiSeq 4000 that was purchased with funds from the National Institutes of Health (NIH) under award no. 1S10OD018220. Sequencing that was generated on an Illumina NovaSeq was supported by the Chan Zuckerberg Biohub. Some of the computing for this project was performed on the Sherlock cluster. Sequencing of the ChIP-seq libraries was supported by the UCSF Center for Advanced Technology. We thank Stanford University and the Stanford Research Computing Center for providing computational resources and support that contributed to these research results. Support for D.C. was provided by National Library of Medicine training grant no. T15LM007033. A. Mezger is supported by the Swedish Research Council (grant no. 2015-06403). F.B. was supported by the Care-for-Rare Foundation and NIH/National Institute of General Medical Sciences funding for the HIV Accessory & Regulatory Complexes Center (no. P50 GM082250; A.Marson). This work was supported by NIH grants (no. 1R01HG008140—J.P. serves as principal investigator with subcontract to A. Marson and L.A.C. at UCSF; no. P30AR071055 to L.A.C.; no. DP3DK111914-01 to A. Marson; no. P50HG007735 to W.J.G.; no. UM1HG009442 to W.J.G.; no. U19AI057266 to W.J.G.), the Howard Hughes Medical

Institute (J.K.P.), the Rheumatology Research Foundation (L.A.C.), the UCSF-Stanford Arthritis Center of Excellence (L.A.C.) (supported in part by the Arthritis Foundation), the Rita Allen Foundation (W.J.G.), the Human Frontiers Science Program grant no. RGY006S (W.J.G.), the Burroughs Wellcome Fund (A. Marson) and the National Multiple Sclerosis Society (A. Marson; no. CA 1074-A-21). Both W.J.G. and A. Marson are supported by the Chan Zuckerberg Biohub. Additionally, A. Marson holds a Career Award for Medical Scientists from the Burroughs Wellcome Fund, has received funding from the Innovative Genomics Institute and is supported by the Parker Institute for Cancer Immunotherapy.

Author contributions

D.C., M.L.T.N., A. Mezger, L.A.C., W.J.G., A. Marson and J.K.P. conceptualized the study. M.L.T.N., A. Mezger, A.K., V.N., N.L., B.W., J.T., F.B. and A.V.P. carried out the investigation. D.C., F.M., D.A.K., Z.G. and J.V.R. carried out the formal analysis. A.K. and F.M. contributed equally to merit second authorship. M.S.A., T.D.B., W.J.G., A. Marson and J.K.P. were responsible for obtaining the resources. L.A.C., W.J.G., A. Marson and J.K.P. acquired the funding. D.C., M.L.T.N. and A. Mezger wrote the original draft. D.C., M.L.T.N., A. Mezger, L.A.C., W.J.G., A. Marson and J.K.P. reviewed and edited the draft. L.A.C., W.J.G., A. Marson and J.K.P. supervised the study.

Competing interests

Stanford University has filed a provisional patent application on the methods described and W.J.G. is named as an inventor. W.J.G. is a cofounder of Epinomics and consultant for 10x Genomics and Guardant Health. A. Marson is a cofounder of Arsenal Biosciences and Spotlight Therapeutics. A. Marson serves as on the scientific advisory board of PACT Pharma, is an advisor to Trizell and was a former advisor to Juno Therapeutics. The Marson Laboratory has received sponsored research support from Juno Therapeutics, Epinomics, Sanofi and a gift from Gilead.

Additional information

Supplementary information is available for this paper at <https://doi.org/10.1038/s41588-019-0505-9>.

Correspondence and requests for materials should be addressed to L.A.C., W.J.G., A.M. or J.K.P.

Reprints and permissions information is available at www.nature.com/reprints.

Publisher's note Springer Nature remains neutral with regard to jurisdictional claims in published maps and institutional affiliations.

© The Author(s), under exclusive licence to Springer Nature America, Inc. 2019

Methods

Data collection. Sample collection and processing. This study was approved by the University of California, San Francisco (UCSF) Committee on Human Research and written consent was obtained from all donors. PBMCs were isolated from whole blood (approximately 450 ml) using Ficoll-Paque PLUS (GE Healthcare Life Sciences) centrifugation. Bulk populations of CD4⁺ T cells, B cells and monocytes were positively enriched, whereas pan-T cells, NK cells and dendritic cells were negatively enriched using magnetic beads before sorting (STEMCELL Technologies). Different cell subsets were sorted on FACS Aria I, FACS Aria II and Fusion flow cytometers (BD Biosciences) up to >95% purity (Supplementary Table 1). Sorted cells were washed once in PBS and were cryopreserved in BAMBANKER freezing medium (Lymphotec) for the ATAC-seq experiments and in TRI reagent (Sigma-Aldrich) for the RNA-seq experiments. Cells frozen in BAMBANKER freezing medium were stored in liquid nitrogen until ready to use. Cells frozen in TRI reagent were stored at -80 °C until further use.

Ex vivo activation. Freshly sorted cells were cultured in Roswell Park Memorial Institute 1640 medium supplemented with glutamine, sodium pyruvate, penicillin-streptomycin, nonessential amino acid and 10% FCS (Sigma-Aldrich). T lymphocytes were stimulated for 24 h with antihuman CD3/CD28 Dynabeads (Thermo Fisher Scientific) at a 1:1 cell-to-bead ratio and human IL-2 (300 U ml⁻¹ for regulatory T cells (T_{reg}), 50 U ml⁻¹ for other T lymphocytes; UCSF Pharmacy). B lymphocytes were activated for 24 h with 10 μg ml⁻¹ F(ab)² antihuman IgG/IgM (Affymetrix) and 20 ng ml⁻¹ human IL-4 (Cell Sciences). NK cells were activated using 2 conditions: (1) with the NK Cell Activation/Expansion Kit according to the manufacturer's instructions for 48 h (Miltenyi Biotec); and (2) with 500 U human IL-2 for 24 h. Monocytes were stimulated with 100 ng ml⁻¹ and 1 μg ml⁻¹ lipopolysaccharide (Sigma-Aldrich) for 6 h and 24 h, respectively. The detailed activation conditions are listed in Supplementary Table 1. After stimulation, cells were washed once with PBS, cryopreserved in BAMBANKER freezing medium and TRI reagent, and stored in liquid nitrogen until ready to use.

RNA-seq library preparation. Cells frozen in TRI reagent were thawed at room temperature for 10 min. Technical replicates were done for each cell aliquot; 100 μl chloroform was added to 500 μl of sample, mixed, incubated at room temperature for 10 min and centrifuged at 12,000 g for 10 min at 4 °C. The aqueous phase was transferred to a new tube and an equal volume of 100% ethanol was added. For further RNA extraction, the Direct-zol RNA MicroPrep Kit (Zymo Research) was used. Samples were mixed thoroughly before transferring onto a Zymo-Spin Ion Chromatography Column and RNA was extracted according to the manufacturer's protocol starting at step 2. RNA-seq library preparation was based on the Smart-seq2 protocol⁵². For oligo deoxythymine annealing, 2 μl of RNA was mixed with 1 μl of recombinant RNase inhibitor (Takara Bio), 1 μl of 10 μM oligo deoxythymine (Integrated DNA Technologies) and 1 μl of 10 mM deoxynucleoside triphosphates (New England Biolabs), and incubated at 72 °C for 3 min. Reverse transcription and template switching were done in 1× First-Strand synthesis buffer (Thermo Fisher Scientific), 100 U SuperScript II reverse transcriptase (Thermo Fisher Scientific), 10 U RNase inhibitor, 5 mM dithiothreitol, 1 M Betaine (Sigma-Aldrich), 6 mM MgCl₂ and 1 μM template-switching oligo (Integrated DNA Technologies). The mixture was incubated at 42 °C for 90 min, 10 cycles of 50 °C for 2 min and 42 °C for 2 min, followed by a final incubation of 15 min at 70 °C. Transcribed RNA was amplified in 1× KAPA HiFi HotStart ReadyMix (Kapa Biosystems), 0.1 μM invading stacking (IS) primer and 0.6× SYBR Green (Thermo Fisher Scientific) as follows: 98 °C for 3 min; 18 cycles of 98 °C for 20 s; 67 °C for 15 s; followed by a final extension at 72 °C for 5 min. Samples were purified using AMPure XP beads (Beckman Coulter Life Sciences) at a 1:1 ratio. Tagmentation of amplified complementary DNA was carried out using the Nextera XT DNA Library Kit (Illumina). In a 20 μl reaction, 150–200 pg cDNA was added to 1× tagmentation DNA buffer (Illumina) and 5 μl of Amplicon Tagmentation Mix (Illumina). The mixture was incubated at 55 °C for 5 min. Then 5 μl of Neutralize Tagment buffer was added to the mixture to stop the fragmentation reaction and incubated for 5 min at room temperature. Tagmented libraries were further amplified in a total reaction volume of 50 μl by adding 15 μl of Nextera PCR Master Mix (Illumina) and 1.25 μM of each, i7 and i5, custom Nextera barcoded PCR primers⁵³ for 3 min at 72 °C, 30 s at 95 °C and 12 cycles of 10 s at 95 °C, 30 s at 55 °C and 30 s at 72 °C. Amplified libraries were purified with AMPure XP beads using a 1:1 ratio.

ATAC-seq library preparation. ATAC-seq libraries were prepared according to the Fast-ATAC protocol¹⁹. In detail, frozen cells were thawed in a water bath, resuspended in 2 ml media and centrifuged at 500g for 5 min. Pelleted cells were resuspended in 1 ml and counted using a hemocytometer. For the ATAC reaction, we took aliquots of 10,000 live cells, unless limited by cell number. Technical replicates were done for all samples. Cells were spun down at 4 °C at 500g for 5 min, washed once in cold PBS and resuspended in the Tn5 reaction buffer (1× tagmentation DNA buffer, 50 μl tagment DNA enzyme 1 Tn5 transposase (Illumina) per ml Tn5 reaction buffer and 0.01% digitonin); 5,000–10,000 cells were transposed in 50 μl of reaction buffer. The reaction volume of samples containing fewer than 5,000 cells was linearly scaled to the number of cells present whereby, for example, 4,000 cells were done in a 40 μl reaction and 2,500 cells were

done in a 25 μl reaction. The Tn5 reaction mix was incubated at 37 °C for 30 min at 300 r.p.m. Transposed samples were purified using MinElute PCR purification columns according to the manufacturer's protocol (QIAGEN). Purified samples were amplified and indexed using custom Nextera barcoded PCR primers (Supplementary Table 1) as described in Buenrostro et al.¹⁸. Amplified libraries were purified using MinElute PCR purification columns.

DNA sequencing. To circumvent index hopping, subpools of samples were created, ran over a 2.5% agarose gel and size-selected, excluding high-molecular-weight DNA, free PCR primers and primer dimers. Samples were purified using a MinElute Gel Purification Kit according to the manufacturer's instructions (QIAGEN). Before sequencing, samples were amplified in 1× NEBNext Master Mix (New England Biolabs), 1.25 μM oligo C (Illumina P5) and 1.25 μM oligo D (Illumina P7) using the following cycle conditions: 30 s at 98 °C followed by 3–4 cycles of 10 s at 98 °C, 30 s at 63 °C and 1 min at 72 °C. All samples were purified using MinElute PCR purification columns. Samples run on the NovaSeq 6000 system were additionally purified using 1× AMPure XP beads to remove free oligo C and D primers. ATAC-seq samples were sequenced on a HiSeq 4000 (Illumina) in paired-end 76 base pair (bp) cycle mode or on a NextSeq 500 (Illumina), without prior gel cleanup, in paired-end 76-bp cycle, high output mode. RNA-seq (cDNA) libraries were either sequenced on a NovaSeq 6000 using a S2 flow cell in paired-end 100-bp cycle mode or on a HiSeq 4000 in paired-end 76-bp cycle mode.

Genotyping. Three hundred microliters of donor blood (donors 1001, 1002, 1003 and 1004) was used to extract genomic DNA using the DNeasy Blood and Tissue Kits (QIAGEN) according to the manufacturer's protocol. We genotyped 958,497 markers using the Infinium OmniExpressExome-8 v1.4 Kit (Illumina). We phased and imputed all biallelic common variants (minor allele frequency > 1%) using the Michigan imputation server that ran Minimac3 with 1,000 G Phase 3 v5 as the reference genome and Eagle v.2.3 (ref.⁵⁴). All genotypes with an imputed heterozygous probability of ≥0.9 were included in downstream allele-specific chromatin accessibility analysis.

Additional details regarding data collection can be found in the Supplementary Note.

Data analysis. RNA-seq. We trimmed the remaining transposase adapters with Cutadapt v.1.13 with a -minimum-length of 20 and an -overlap of 5 in paired-end mode⁵⁵. RNA-seq reads were pseudoaligned using Kallisto v.0.43.0 (ref.⁵⁶). The Kallisto index was made with default parameters and the GENCODE (release 25, lift 37) FASTA file⁵⁷ and was run in quant mode with default parameters. Following pseudoalignment, we computed gene abundances using tximport v.1.2.0 (ref.⁵⁸). We excluded donor cell type samples with fewer than one million total reads from all technical replicates or that were extreme principal component analysis (PCA) outliers. Discarded cell types include thymocyte subsets and TECs.

ATAC-seq. We trimmed the remaining transposase adapters with Cutadapt v.1.13 with a -minimum-length of 20 and an -overlap of 5 in paired-end mode⁵⁵. We aligned ATAC-seq reads using Bowtie 2 v.2.2.9 with default parameters and a maximum paired-end insert distance of 2 kbp. The Bowtie 2 index was constructed with the default parameters for the hg19 reference genome. We filtered out reads that mapped to chromosome M and used SAMtools v.1.4 to filter out reads with mapping quality < 30 and with the flags '-F 1804' and '-f 2'. Additionally, duplicate reads were discarded using Picard Tools v.1.134 (<http://broadinstitute.github.io/picard/>). We calculated the percentage aligning to mitochondria, the percentage within blacklist regions⁵⁹ and the enrichment of reads at transcription start site (TSS) regions relative to 2 kb away using the RefSeq gene annotation (referred to elsewhere as TSS enrichment). Chromatin accessibility peaks were identified with MACS2 v.2.1.1 under default parameters and '-nomodel -nolambda -keep-dup all -call-summits'. The count of absolute peaks per cell type refers to the number of peak regions reported in the 'narrowPeak' file (peaks with multiple summits are only counted once). We reported the peak count estimate after linearly adjusting for estimated confounding effects from sample read depth and TSS enrichment (a proxy for sample quality). A consensus set of peaks was defined by merging overlapping (≥1 bp) peaks identified in at least two samples across all samples. This set of peaks had a median peak length of 346 bp following removal of peaks that were >3 kb or nonautosomal. We then used the 'get_count' function from the nucleotATAC Python package to count the number of fragments within the consensus peak set across all samples⁶⁰. We excluded donor samples with fewer than 5 million reads from all technical replicates that passed the quality filters, a TSS enrichment score <4, >0.5% of reads mapping to a known set of blacklist regions⁵⁹, >25% of reads mapping to the mitochondria or that were extreme PCA outliers. We used deepTools v.2.5.1 to generate bigWig tracks with a genomic bin size of 10 bp, reads per kilobase of transcript per million mapped reads (RPKM) normalization and the '-extendReads' parameter.

Differentially expressed genes. For this analysis, we included only unique protein coding genes from GENCODE v.25. Additionally, we eliminated all genes that had below ten counts per million (CPM) in at least two biological replicate samples, resulting in 13,512 genes tested. We used the trimmed mean of *M* values

normalization method to compute scale factors for each sample and voom to compute the weights capturing the relationship between gene expression mean and variance. For each cell type, we used limma to estimate the $\log_2(\text{fold change})$ of gene expression for each gene on stimulation. We included donor in the design matrix to correct for donor-specific effects. We considered a gene differentially expressed if the limma-reported Benjamini–Hochberg-corrected P value⁶¹, which we refer to as a q , was <0.01 and the absolute $\log_2(\text{fold change})$ was >1 .

Differentially accessible chromatin regions. Starting with the consensus peak set, we eliminated all peaks with fewer than 1 CPM in at least two biological replicate samples, resulting in 671,448 tested peaks. We used the trimmed mean of M values method to compute scale factors for each sample and voom to compute the weights capturing the relationship between mean and variance chromatin accessibility across samples. For each cell type, we used limma to estimate the $\log_2(\text{fold change})$ of each chromatin accessibility region on stimulation, while controlling for donor and the enrichment of reads at TSSs (the latter serves as a proxy for sample quality). We considered a region a significant differentially accessible chromatin peak if the limma-reported Benjamini–Hochberg-corrected P value was <0.01 and the estimated absolute $\log_2(\text{fold change})$ from the resting to stimulation condition was >1 . We initially considered different stimulation conditions of NK and monocyte samples separately. However, the estimated $\log_2(\text{fold change})$ stimulation effects were nearly identical among significant stimulation peaks when the conditions were pooled or unpooled (adjusted $R^2=0.88$ for mature NK cells and $R^2=0.99$ for monocytes). Thus, we reported the summary statistics from the pooled differential accessibility analysis.

Quantifying the amount of shared stimulation response. We aimed to quantify the sharing of stimulation effects between two cell types, denoted A and B. To do this we first determined the set of differentially accessible peaks ($q < 0.01$ and $\log_2(\text{fold change}) > 1.0$) from cell type A (using limma-voom; see section on Differentially accessible chromatin regions). For this set of peaks, we computed Pearson's correlation (with the 'cor' function in R) between stimulation effects ($\log_2(\text{fold change})$) in cell type A and B. This analysis resulted in asymmetric sharing estimates conditioning on significant peaks from cell type A or B. We found that the asymmetric estimates were broadly consistent, so we reported the mean correlation weighted by the number of significant peaks in each cell type. Individual asymmetric correlation estimates can be found in Supplementary Table 1.

Allele-specific chromatin accessibility. We collected all aligned reads that overlapped heterozygous sites. Initially, we used the set of heterozygous sites identified with 'HaplotypeCaller' from GATK v.3.7 with '-minPruning 10' and '-stand_call_conf 20' run on a donor-specific BAM file including all samples from the donor⁶². The final set of heterozygous sites that we used for analysis were the intersection of the GATK and genotyped sites passing filters (see section on Genotyping). Next, we passed all aligned reads that overlapped heterozygous sites through WASP filtering³⁹. Briefly, the read was remapped with the SNP allele flipped (we only examined biallelic sites) and was only retained if it mapped to the same location. This filtering approach effectively eliminates reference genome biases enabling unbiased estimation of the proportion of reads mapping to the reference allele. At each heterozygous site we counted the number of WASP-filtered reads mapping to the reference and alternative allele. We computed a P value per heterozygous site using a binomial test, and for each sample corrected for multiple hypotheses by computing Benjamini–Hochberg q values. P values were converted to Benjamini–Hochberg q values using the 'p.adjust' function in R.

Estimating the proportion of shared allele-specific imbalance effects. We first computed the posterior mean and variance of the proportion of reads mapping to the reference allele, assuming a uniform prior on the proportion and a binomial likelihood. The posterior under this model is $\text{Beta}(r + 1, a + 1)$, where r and a are the numbers of reads mapping to the reference and alternative allele, respectively. At each heterozygous site, we defined the effect as the difference between the proportion of reads mapping to the reference and the expectation under the null hypothesis of no allele-specific effect, that is, 50%.

We aimed to estimate the proportion of shared imbalance effects between two cell types, denoted A and B. To do this, we first determined the set of significant ASC sites ($q < 0.01$) from cell type A (see section on Allele-specific chromatin accessibility). We collected the effects and variances for these ASC sites in cell type B and then used ashR v.2.2-7 (ref. ⁴⁰) to estimate the proportion of these effects that are nonzero. While comparable methods, such as Storey's pi1, only use P values⁶³, ashR leverages both effect size and s.e.m. estimates to improve power. We reported the average sharing estimates; however, individual values can be found in Supplementary Table 1.

GWAS and eQTL enrichments. To identify genomic annotations enriched for genetic trait heritability, we used LD Score regression v.1.0.0 under the partitioning heritability mode with default parameters. We excluded SNPs from the major histocompatibility complex region for this analysis. To assess enrichment of rheumatoid arthritis signal in ASC sets, we compared against the distribution of the P values for the rheumatoid arthritis GWAS genome-wide (the same summary statistics that were used in the LD Score analysis). To assess enrichment of blood eQTL signal in the ASC sets, we compared against the distribution of P values from all variant-gene pairs available.

Additional details regarding data analysis can be found in the Supplementary Note.

Reporting Summary. Further information on research design is available in the Nature Research Reporting Summary linked to this article.

Data availability

Our RNA-seq, ATAC-seq and ChIP-seq data have been deposited with the Gene Expression Omnibus (GEO): RNA-seq data (accession no. GSE118165); ATAC-seq data (accession no. GSE118189); ChIP-seq data (accession no. GSE126505). Progenitor data have been deposited with the GEO under accession no. GSE74912. Additional supplementary information can be retrieved from the Pritchard Lab Data website (<http://web.stanford.edu/group/pritchardlab/dataArchive.html>).

References

- Picelli, S. et al. Full-length RNA-seq from single cells using Smart-seq2. *Nat. Protoc.* **9**, 171–181 (2014).
- Buenrostro, J. D. et al. Single-cell chromatin accessibility reveals principles of regulatory variation. *Nature* **523**, 486–490 (2015).
- Das, S. et al. Next-generation genotype imputation service and methods. *Nat. Genet.* **48**, 1284–1287 (2016).
- Martin, M. Cutadapt removes adapter sequences from high-throughput sequencing reads. *EMBnet J.* **17**, 10–12 (2011).
- Bray, N. L., Pimentel, H., Melsted, P. & Pachter, L. Near-optimal probabilistic RNA-seq quantification. *Nat. Biotechnol.* **34**, 525–527 (2016).
- Harrow, J. et al. GENCODE: the reference human genome annotation for The ENCODE Project. *Genome Res.* **22**, 1760–1774 (2012).
- Soneson, C., Love, M. I. & Robinson, M. D. Differential analyses for RNA-seq: transcript-level estimates improve gene-level inferences. *F1000Res.* **4**, 1521 (2015).
- Dunham, I. et al. An integrated encyclopedia of DNA elements in the human genome. *Nature* **489**, 57–74 (2012).
- Schep, A. N. et al. Structured nucleosome fingerprints enable high-resolution mapping of chromatin architecture within regulatory regions. *Genome Res.* **25**, 1757–1770 (2015).
- Benjamini, Y. & Hochberg, Y. Controlling the false discovery rate: a practical and powerful approach to multiple testing. *J. R. Stat. Soc. Series B Stat. Methodol.* **57**, 289–300 (1995).
- McKenna, A. et al. The Genome Analysis Toolkit: a MapReduce framework for analyzing next-generation DNA sequencing data. *Genome Res.* **20**, 1297–1303 (2010).
- Storey, J. D. & Tibshirani, R. Statistical significance for genomewide studies. *Proc. Natl Acad. Sci. USA* **100**, 9440–9445 (2003).

Reporting Summary

Nature Research wishes to improve the reproducibility of the work that we publish. This form provides structure for consistency and transparency in reporting. For further information on Nature Research policies, see [Authors & Referees](#) and the [Editorial Policy Checklist](#).

Statistics

For all statistical analyses, confirm that the following items are present in the figure legend, table legend, main text, or Methods section.

n/a Confirmed

- The exact sample size (n) for each experimental group/condition, given as a discrete number and unit of measurement
- A statement on whether measurements were taken from distinct samples or whether the same sample was measured repeatedly
- The statistical test(s) used AND whether they are one- or two-sided
Only common tests should be described solely by name; describe more complex techniques in the Methods section.
- A description of all covariates tested
- A description of any assumptions or corrections, such as tests of normality and adjustment for multiple comparisons
- A full description of the statistical parameters including central tendency (e.g. means) or other basic estimates (e.g. regression coefficient) AND variation (e.g. standard deviation) or associated estimates of uncertainty (e.g. confidence intervals)
- For null hypothesis testing, the test statistic (e.g. F , t , r) with confidence intervals, effect sizes, degrees of freedom and P value noted
Give P values as exact values whenever suitable.
- For Bayesian analysis, information on the choice of priors and Markov chain Monte Carlo settings
- For hierarchical and complex designs, identification of the appropriate level for tests and full reporting of outcomes
- Estimates of effect sizes (e.g. Cohen's d , Pearson's r), indicating how they were calculated

Our web collection on [statistics for biologists](#) contains articles on many of the points above.

Software and code

Policy information about [availability of computer code](#)

Data collection

Data analysis

For manuscripts utilizing custom algorithms or software that are central to the research but not yet described in published literature, software must be made available to editors/reviewers. We strongly encourage code deposition in a community repository (e.g. GitHub). See the Nature Research [guidelines for submitting code & software](#) for further information.

Data

Policy information about [availability of data](#)

All manuscripts must include a [data availability statement](#). This statement should provide the following information, where applicable:

- Accession codes, unique identifiers, or web links for publicly available datasets
- A list of figures that have associated raw data
- A description of any restrictions on data availability

Our GEO RNA-seq data repository: GSE118165
 Our GEO ATAC-seq data repository: GSE118189
 Our GEO ChIP-seq data repository: GSE126505
 Progenitor data GEO accession: GSE74912
 Additional supplementary information: <http://web.stanford.edu/group/pritchardlab/dataArchive.html>

Field-specific reporting

Please select the one below that is the best fit for your research. If you are not sure, read the appropriate sections before making your selection.

Life sciences Behavioural & social sciences Ecological, evolutionary & environmental sciences

For a reference copy of the document with all sections, see [nature.com/documents/nr-reporting-summary-flat.pdf](https://www.nature.com/documents/nr-reporting-summary-flat.pdf)

Life sciences study design

All studies must disclose on these points even when the disclosure is negative.

Sample size	We aimed to collect at least 3 biological samples for each cell subset. This number was chosen to balance power and the costs of collecting many diverse cell subsets.
Data exclusions	The quality of the RNA-seq data collected from the thymocytes was lacking, and so we excluded these samples from our study.
Replication	Most biological samples had technical replicates.
Randomization	Samples were randomly allocated.
Blinding	The investigators were blinded to group allocation.

Reporting for specific materials, systems and methods

We require information from authors about some types of materials, experimental systems and methods used in many studies. Here, indicate whether each material, system or method listed is relevant to your study. If you are not sure if a list item applies to your research, read the appropriate section before selecting a response.

Materials & experimental systems

n/a	Included in the study
<input type="checkbox"/>	<input checked="" type="checkbox"/> Antibodies
<input checked="" type="checkbox"/>	<input type="checkbox"/> Eukaryotic cell lines
<input checked="" type="checkbox"/>	<input type="checkbox"/> Palaeontology
<input checked="" type="checkbox"/>	<input type="checkbox"/> Animals and other organisms
<input type="checkbox"/>	<input checked="" type="checkbox"/> Human research participants
<input checked="" type="checkbox"/>	<input type="checkbox"/> Clinical data

Methods

n/a	Included in the study
<input type="checkbox"/>	<input checked="" type="checkbox"/> ChIP-seq
<input type="checkbox"/>	<input checked="" type="checkbox"/> Flow cytometry
<input checked="" type="checkbox"/>	<input type="checkbox"/> MRI-based neuroimaging

Antibodies

Antibodies used	We have updated supplemental table excel file with the relevant information about the antibodies we used.
Validation	Antibody validations were performed by suppliers.

Human research participants

Policy information about [studies involving human research participants](#)

Population characteristics	Healthy human blood donors were female or male between the ages of 21 and 50.
Recruitment	Fresh blood was taken from healthy human donors under a protocol approved by the UCSF Committee on Human Research (CHR#13-11950). All donors provided informed consent. Human thymus was obtained from 18- to 22-gestational-week specimens under the guidelines of the University of California San Francisco Committee on Human Research
Ethics oversight	UCSF Committee on Human Research

Note that full information on the approval of the study protocol must also be provided in the manuscript.

ChIP-seq

Data deposition

- Confirm that both raw and final processed data have been deposited in a public database such as [GEO](#).
- Confirm that you have deposited or provided access to graph files (e.g. BED files) for the called peaks.

Data access links

May remain private before publication.

For "Initial submission" or "Revised version" documents, provide reviewer access links. For your "Final submission" document, provide a link to the deposited data.

Files in database submission

Provide a list of all files available in the database submission.

Genome browser session

(e.g. [UCSC](#))

Provide a link to an anonymized genome browser session for "Initial submission" and "Revised version" documents only, to enable peer review. Write "no longer applicable" for "Final submission" documents.

Methodology

Replicates

Describe the experimental replicates, specifying number, type and replicate agreement.

Sequencing depth

Describe the sequencing depth for each experiment, providing the total number of reads, uniquely mapped reads, length of reads and whether they were paired- or single-end.

Antibodies

Describe the antibodies used for the ChIP-seq experiments; as applicable, provide supplier name, catalog number, clone name, and lot number.

Peak calling parameters

Specify the command line program and parameters used for read mapping and peak calling, including the ChIP, control and index files used.

Data quality

Describe the methods used to ensure data quality in full detail, including how many peaks are at FDR 5% and above 5-fold enrichment.

Software

Describe the software used to collect and analyze the ChIP-seq data. For custom code that has been deposited into a community repository, provide accession details.

Flow Cytometry

Plots

Confirm that:

- The axis labels state the marker and fluorochrome used (e.g. CD4-FITC).
- The axis scales are clearly visible. Include numbers along axes only for bottom left plot of group (a 'group' is an analysis of identical markers).
- All plots are contour plots with outliers or pseudocolor plots.
- A numerical value for number of cells or percentage (with statistics) is provided.

Methodology

Sample preparation

Describe the sample preparation, detailing the biological source of the cells and any tissue processing steps used.

Instrument

Identify the instrument used for data collection, specifying make and model number.

Software

Describe the software used to collect and analyze the flow cytometry data. For custom code that has been deposited into a community repository, provide accession details.

Cell population abundance

Describe the abundance of the relevant cell populations within post-sort fractions, providing details on the purity of the samples and how it was determined.

Gating strategy

Describe the gating strategy used for all relevant experiments, specifying the preliminary FSC/SSC gates of the starting cell population, indicating where boundaries between "positive" and "negative" staining cell populations are defined.

- Tick this box to confirm that a figure exemplifying the gating strategy is provided in the Supplementary Information.